28 May 2010, 5:30 pm - 6:15 pm

Calibrated 3D Computational Modeling of Soil-Structure Systems and Liquefaction Scenarios

Ahmed Elgamal

University of California San Diego, La Jolla, CA

Fifth International Conference on
Recent Advances in Geotechnical Earthquake Engineering and Soil Dynamics
and Symposium in Honor of Professor I.M. Idriss
May 24-29, 2010 • San Diego, California

CALIBRATED 3D COMPUTATIONAL MODELING OF SOIL-STRUCTURE SYSTEMS AND LIQUEFACTION SCENARIOS

Ahmed Elgamal
Univ. of California, San Diego
La Jolla, CA 92093

ABSTRACT

Three-dimensional (3D) computational simulation is increasingly allowing for insights into the mechanics of seismic soil-structure system response. Calibration is being facilitated by field, full-scale, and centrifuge model laboratory data. Computational algorithms and scenario-specific graphical user-interfaces are gradually permitting the routine adoption of such geometrically realistic simulation environments. This paper presents an overview of salient recent 3D soil-foundation-structure earthquake response simulations.

Developments related to graphical user-interfaces (OpenSeesPL, http://cyclic.ucsd.edu/openseespl) are summarized, demonstrating the current and evolving capabilities towards performance-based earthquake engineering (PBEE). From an OpenSeesPL-generated lateral push-over analysis of a large pile-group, it is shown that corner piles may shoulder a significantly higher level of load (axial, shear, and bending). Evolution of large tensile forces in these piles may warrant careful consideration. Modeling of liquefaction response mechanisms are also discussed, highlighting the role of cyclic mobility and influence of permeability in dictating the level of associated ground shear deformations, and related countermeasure performance.

INTRODUCTION

Soil-structure interaction (SSI) effects play a major role in dictating the response of structures to earthquakes. In order to satisfactorily reproduce these SSI effects, it is often of interest to represent the geometry of the entire ground-foundation-structural system. The need for high spatial/temporal resolution is an additional challenge when analyzing such models. With the developments in material modeling techniques and high-speed efficient computers, linear and nonlinear three-dimensional (3D) finite-element (FE) methods are becoming a promising technique for understanding these SSI mechanisms.

Particularly suited to seismic applications, the open-source computational platform OpenSees (Mazzoni et al. 2006, http://opensees.berkeley.edu) provides such 3D simulation capabilities. In order to facilitate the pre- and post-processing phases, a recently developed graphical user interface OpenSeesPL facilitates the execution of 3D push-over and seismic footing/pile-ground simulations (Lu et al. 2006, http://cyclic.ucsd.edu/openseespl/). Various ground modification scenarios may be also studied by appropriate specification of the material within the pile zone.

In the following sections, an overview of two recent ground-foundation-structure simulations is presented, with emphasis on the insights gained from such system-level analyses. Capabilities of scenario-specific graphical user interfaces for routine 3D analysis of ground-pile systems are then briefly discussed. From a large 3D pile-group lateral push-over analysis, it is shown that corner piles may shoulder a significantly higher level of load (axial, shear, and bending). Ongoing user-interface developments for performing a full-probabilistic performance-based earthquake engineering analysis are also highlighted.

Thereafter, attention is shifted towards liquefaction-induced lateral ground deformation, and the combined roles of cyclic mobility and soil permeability. On this basis, use of 3D simulation for modeling of liquefaction countermeasures (stone columns and pile-pinning) is finally addressed.

3D SYSTEM-LEVEL SIMULATIONS

The continued advances in computational software and hardware are now permitting the systematic use of three-dimensional (3D) simulation for a wide class of geotechnical

earthquake engineering applications. Numerical modeling of soil-foundation-structure seismic response is increasingly generating valuable insights. System as well as component behavior reveal mechanisms that may qualitatively and quantitatively influence the state of practice and design. Potential seismically-induced ground deformation effects are systematically imposed along with the loads due to dynamic excitation. In such scenarios, high fidelity simulations are permitted by large-scale three-dimensional modeling. Pre- and post-processing and visualization tools are also an integral component.

I. Bridge-Foundation-Ground System

The Humboldt Bay Middle Channel Bridge near Eureka in northern California (Yan 2006) is a Testbed that motivated seismic computational simulation efforts of entire ground-structure systems (Elgamal et al. 2008). Initiated by the Pacific Earthquake Engineering Research (PEER) center, this Testbed serves as an environment for integration of the overall research outcomes and objectives. The bridge (Figs. 1, 2) is a 330m long, 9-span structure, supported on the cap beams of single pier bents with both longitudinal and transversal shear keys to prevent unseating. Below the bridge, average slope of the river channel from the banks to its center is about 7% (4 degrees).

Figure 1. Humboldt Bay bridge (from Elgamal et al. 2008).

Initially, 2D studies were undertaken (Zhang et al. 2008), followed by a full 3D investigation (Yan 2006, Elgamal et al. 2008). The Finite Element (FE) nonlinear solution was conducted using the PEER open-source software platform OpenSees (http://opensees.berkeley.edu, Mazzoni et al. 2006). This FE model included 30237 nodes, 1140/280 linear/nonlinear beam-column elements (Figure 3), 81 linear shell elements, 23556 solid brick elements, 1806 zero-length elements, and 2613 equalDOF constraints. The simulated soil domain (Figure 3) is 650 m long, 151 m wide and 74.5 m deep.

In this study, a nonlinear elasto-plastic multi-yield surface J_2 soil model was employed. Nonlinear fiber elements were used to model the bridge piers and piles (further details are provided in the Appendix). The September 16, 1978 Tabas earthquake record was employed to derive a vertically incident earthquake motion along the FE mesh base using deconvolution techniques (Yan 2006). For that purpose, a protocol for handling the base boundary condition was careful defined and executed (to permit staged loading in terms of application of own weight of the ground and structure, transition to the nonlinear material models, and imparting the incident wave ground motion). As such, the development strategy for this 3D ground-foundation-structure FE mesh (Fig. 3) involved:

i) Representation of the essential structural and foundation elements of the bridge (Fig. 2). In this regard, the foundation under each pier was modeled by a 2x2 pile group. Stiff strengthened zones were included below the bridge approach ramps (Fig. 4).

ii) Placement of the mesh lateral and vertical boundaries as far away as possible from the bridge, its foundation, and approach ramps.

iii) Employment of the largest possible FE mesh within the limitation of in-core execution of the computations on a 32 bit Windows-based Personal Computer. In this mesh, the soil elements were configured to be relatively small around the bridge and its foundation, becoming gradually larger towards the outer mesh boundaries (Fig. 3).

iv) Provision for exploring the impact of permanent ground deformation, by inclusion of a realistic relatively soft soil stratum at shallow depth traversing the bridge site and its underlying waterway (Yan 2006, Elgamal et al. 2008).

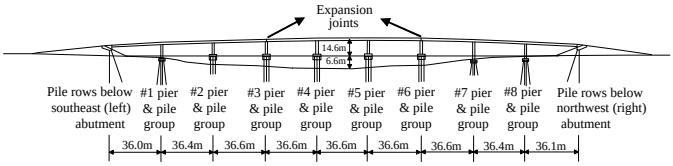

Figure 2. Schematic of bridge, pile foundations,and approach ramps (from Elgamal et al. 2008).

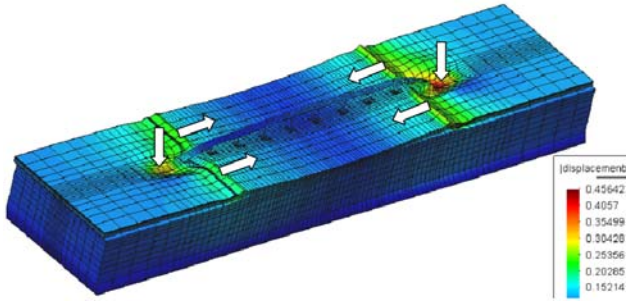

Figure 3. 3D bridge and soil layers (Yan 2006).

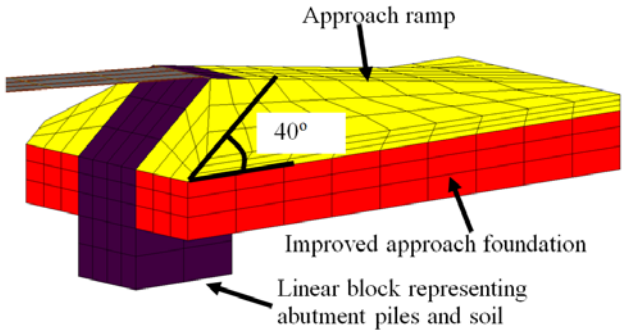

Figure 4. Abutment and approach ramp zone (Yan 2006).

Among the main observations from this study are:
1) Permanent ground deformation can have a major impact on the overall bridge deformation pattern (Fig. 5). Translation of the pile groups towards the center of the underlying waterway (Fig. 5) may induce significant moments and shear forces in the bridge piers.
2) Settlement and lateral translation of the approach ramps and bridge abutments (Fig. 3) may induce very large destructive forces into the bridge super-structure (Fig. 5).

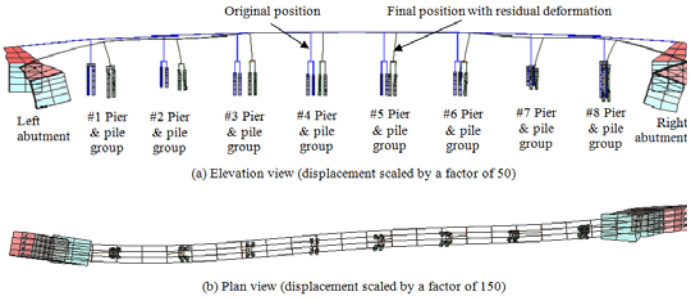

Figure 5. Elevation and plan views of the bridge system after earthquake shaking (Yan 2006).

II. Wharf on Piles

Wharfs supported on piles are common Port structures in the United States. The seismic response involves significant pile-slope interaction that is best simulated by modelling the actual 3D configuration. To address this issue, a 3D idealized model of a pile-supported wharf system was studied (Lu 2006). The idealized geometric model (Figure 6) is based on typical configurations of pile-supported wharf structures (Berth 100 Container Wharf at the Port of Los Angeles).

In Figure 6, a 3D slice in this wharf system (central zone) is shown, that exploits symmetry of the supporting pile-system configuration (Lu 2006). This slice is supported by a total of 16 piles in 6 rows. Each pile is 0.6 m in diameter, and 43 m in length (reinforced concrete). Relative to the piles, the wharf deck was assumed to be essentially rigid (with a thickness of 0.8 m).

Two soil layers were represented in this idealized model. The lower layer (25 m in thickness) was modelled as stiff clay (255 kPa of *Cohesion*) and the upper layer a weaker medium-strength clay (44 kPa of *Cohesion*), with a slope inclination of about 39 degrees. Water table level was located at 16.6 m above the mud-line.

The base of the FE model was assumed rigid, and a scaled Rinaldi Receiving Station record from the 1994 Northridge Earthquake was employed as the base input motion. On the waterside and landside of this FE model, motion was specified as the computed accelerations from a one-dimensional (1D) shear beam simulation (Yang et al. 2004) of the left and right soil columns. Symmetry along the front and back side boundaries was represented by roller supports. A total of 64 processors were employed (parallel implicit integration scheme) in computing the response and the total execution time was about 12 hours.

Figure 6 shows the final deformed mesh of this pile-supported wharf system. As can be seen, the majority of the deformation occurs within the upper layer while the lower soil layer shows insignificant lateral displacement. A pile-pinning effect was observed, where a lower level of lateral deformation occurred (Fig. 6), compared to an additional free-slope (without Wharf or piles) simulation (Lu 2006). Finally, it is seen that slope and pile deformation show a level of uniformity below the entire wharf structure. As such, both front as well as back piles are seen to exhibit a similar pattern of deformation. In essence, displacement of the back piles (nearest to the landside) was not restricted by the slope crest zone, which also translated laterally along with the slope toe sections (precluding the occurrence of a high drift ratio for the back piles).

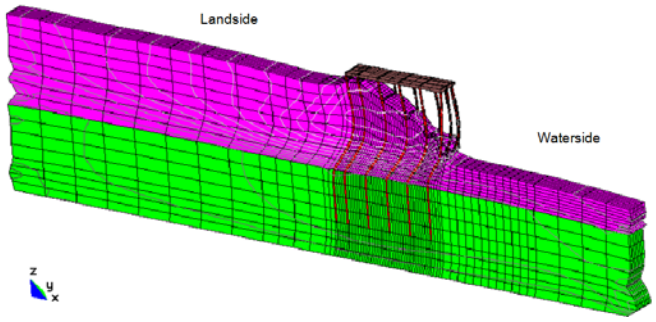

Figure 6. Final deformed mesh (factor of 30) of pile-supported wharf (Lu 2006).

III. Graphical Interfaces to facilitate 3D simulations

In conducting numerical simulations, preparation of the FE input files is a step that requires careful attention. A minor oversight might go undetected, leading to erroneous results. Numerous opportunities for such small errors abound, and a user-friendly interface can significantly alleviate this problem, and allow for high efficiency and much increased confidence. In this regard, a Windows-based graphical-user-interface OpenSeesPL has been initiated for pile-ground interaction analyses (http://cyclic.ucsd.edu/openseespl).

Particularly suited to static as well as seismic applications, the open-source computational platform OpenSees (Mazzoni et al. 2006, http://opensees.berkeley.edu) is employed throughout. In the OpenSees platform, a wide range of linear and nonlinear soil and structural elements is available (details are included in the Appendix).

OpenSeesPL (Figures 7 and 8) allows for the execution of push-over and seismic footing/pile-ground simulations (Lu et al. 2006). Various ground modification scenarios may be also studied by appropriate specification of the material within the pile zone. In summary, OpenSeesPL allows for: i) convenient creation of the mesh, associated boundary conditions, and loading parameters (FE input file), ii) execution of the computations using the OpenSees platform, and iii) graphical display of the results for the footing/pile and the ground system (Fig. 9).

As such, OpenSeesPL is focused on facilitating a wide class of 3D studies (with additional capabilities yet under development). The basic default configuration is in the form of a 3-dimensional soil island with the possibility of including a footing/pile/pile-group model. Full-mesh, half-mesh, or quarter mesh configurations may be analyzed, as dictated by symmetry considerations.

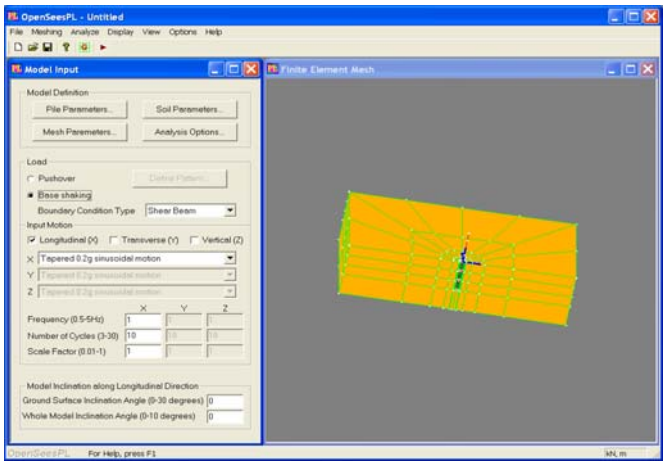

Figure 7. OpenSeesPL user interface showing (1/2 mesh due to uniaxial lateral loading symmetry) a circular pile in level ground (Lu et al. 2006).

In OpenSeesPL, the mesh configuration may be easily modified to: i) change the pile diameter, depth of embedment, height above ground surface and number of pile beam-column elements, and ii) refine the ground mesh domain in the lateral and vertical directions. Square or circular pile cross-sections may be specified. Shallow foundations in square or circular configurations may be also conveniently analyzed.

Independent control over the pile zone material may be exercised, allowing for a wide range of ground modifications studies. Of particular importance and significance in these scenarios is the ability to simulate the presence of a mild infinite-slope configuration, allowing estimates of accumulated ground deformation, efficacy of a deployed liquefaction countermeasure, pile-pinning effects, and liquefaction-induced lateral pile loads and resulting moments/stresses.

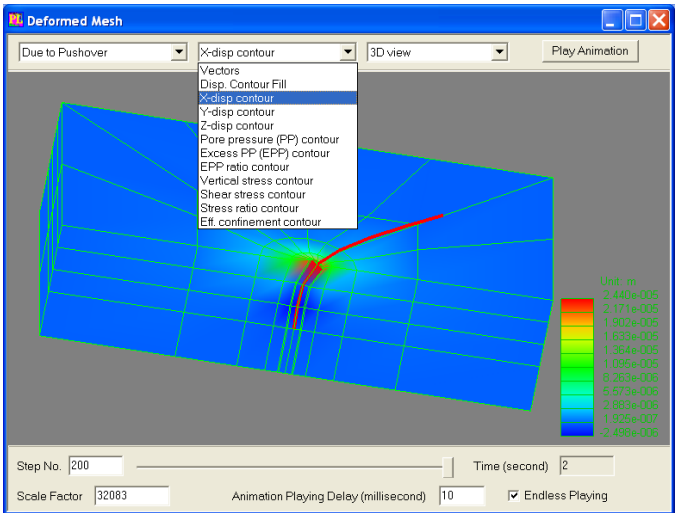

Figure 8. Push-over analysis and deformed mesh window in OpenSeesPL (Lu et al. 2006).

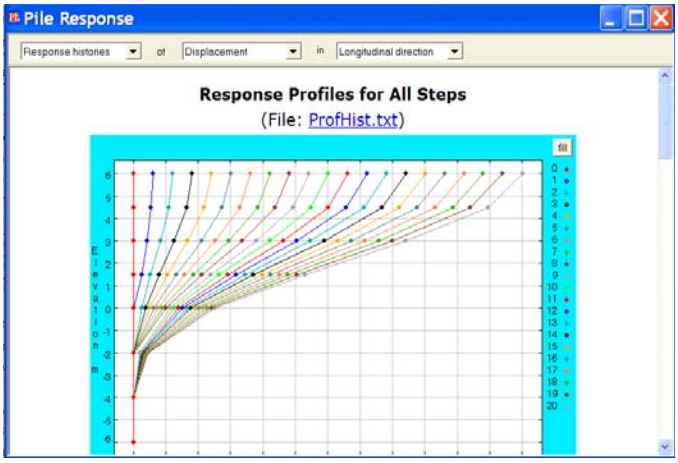

Figure 9. OpenSeesPL pile displacement load-step display (monotonic load).

OpenSeesPL simulation scenarios

III.1. Using OpenSeesPL, Elgamal and Lu (2009) conducted a pilot study of lateral loading on a 3x3 pile group. A single-pile FE model was first calibrated in the linear range based on the 3D analytical solution of Abedzadeh and Pak (2004). Response of this linear pile in an idealized nonlinear undrained-clay material was then computed and compared to the linear solution. The corresponding 3x3 pile group response was also addressed, as a function of pile-spacing for the above linear and nonlinear soil cases (Figures 10 and 11).

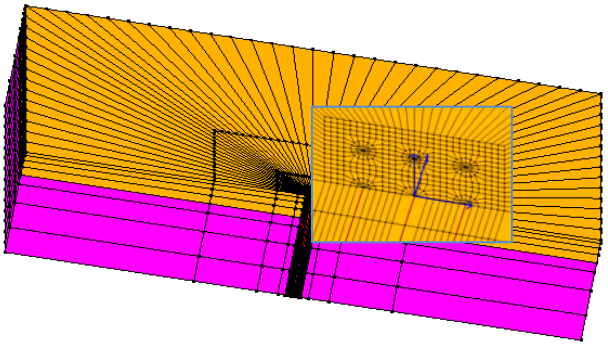

Figure 10. FE mesh of 3x3 pile group -1/2 mesh due to symmetry-(from Elgamal and Lu 2009).

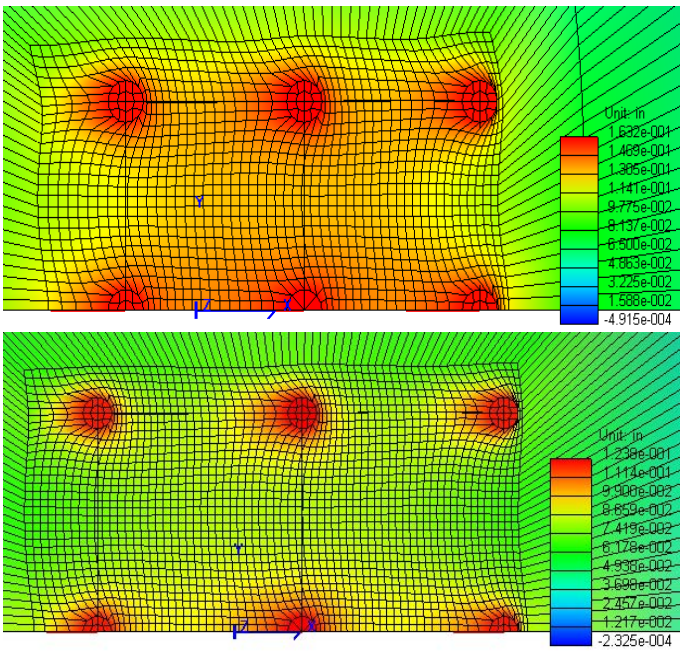

Figure 11. Plan view of displacement around piles for 5 (above) and 7 (below) pile-diameter spacing (1/2 mesh configuration, with red color denoting the large displacement zones).

III.2 Using OpenSeesPL, computational modeling of the response of a large pile group under lateral load was recently conducted (Lu et al. 2010). The pile group is configured in an 8 x 4 arrangement with a longitudinal spacing of 2 pile diameters and a transversal spacing of 2.15 pile diameters on center. Each pile is 1.37 m in diameter and 30.8 m long. The group is rigidly connected by a pile cap 14.3 m above the mudline (Figs. 12, 13).

In view of symmetry, a half mesh configuration was used (Fig. 12). Length of the mesh in the longitudinal direction is 394 m, with 191 m transversally (in this half-mesh configuration, resulting in a 394 m x 382 m soil domain in plan view). Total soil layer thickness was 43.9 m (the base of the soil domain is 27.4 m below the pile tip). The soil domain was modeled by eight-node brick elements (23,040 in total) and the piles were modeled by beam-column elements (512 in total). Rigid beam-column elements (1,664 in total) are used around each pile to model the pile size (diameter). After application of the bridge own weight, a pile cap longitudinal displacement was applied up to a maximum of 0.12 m (allowing the final lateral load to exceed the applied vertical bridge own-weight force).
The final deformed mesh in shown in Fig. 13, along with the stress ratio contour fill (red color shows yielded soil elements). Along with translation, the pile group is seen to also undergo some overall rotation.

In the initial static state, the axial-force share of each pile varied in a wide range. Piles along the circumference carry most of the load with the corner piles shouldering the biggest burden (more than twice that of an equivalent single pile scenario). The inner piles hardly see much of the applied dead load.

At the attained peak lateral displacement (Lu et al. 2010): i) the corner front pile carries the highest portion of shear force and bending moment, ii) the center front pile, and the two back piles also sustain relatively high levels, iii) the inner piles carry the least burden (about 60% of the share of the corner pile, iv) the back piles (particularly the corner pile) experience substantial tensile forces that warrant a careful analysis of the pile and pile-pile cap connection, and v) compression in the corner front-pile more than doubles.

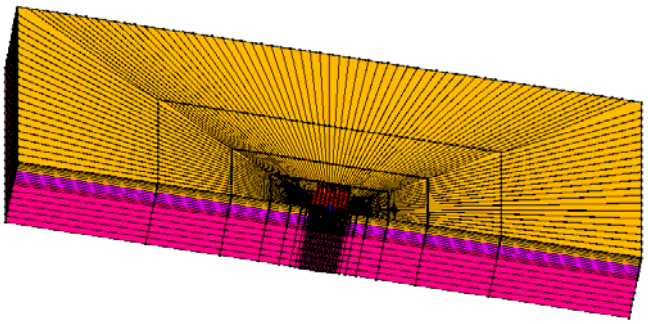

Figure 12. Finite element mesh (Lu et al. 2010).

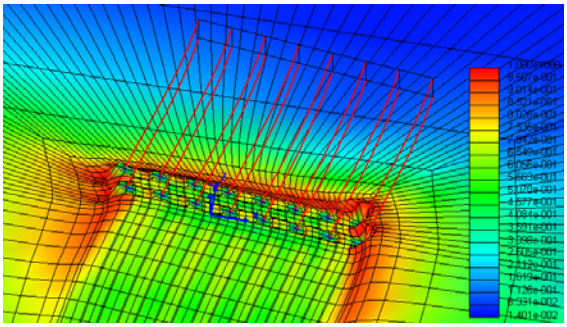

Figure 13. Final deformed mesh (factor of 50): a) stress ratio contour fill -red color shows yielded soil elements- (Lu etal. 2010).

IV. User interface for PBEE

A graphical user interface is under development (collaborative effort by K. Mackie, J. Lu and A. Elgamal) to combine nonlinear dynamic time history analysis of bridge-foundation-ground systems with an implementation of performance-based earthquake engineering (PBEE). The user interface builds upon previous code that allowed for analysis of piles in a soil domain under nonlinear static and nonlinear dynamic loads (OpenSeesPL). Functionality was extended for analysis of multiple suites of ground motions (Figure 14) and combination of results probabilistically using the PEER PBEE framework (Mackie et al. 2008, 2010). Definition of the bridge and underlying ground configuration and material properties is greatly facilitated using this new interface (Figure 15). In addition, all stages of the involved analyses are conveniently executed in a systematic fashion, allowing the end user to investigate typical single-bent bridge configurations.

In the PBEE framework (Mackie et al. 2008, 2010), the response quantities of interest are tied directly to Performance Groups (PGs) that are used for assessing damage and repair (e.g, maximum column drift ratio, abutment pile cap displacement, etc.). Discrete damage states (DS) are defined for the performance groups (Fig. 16), and each DS is associated with a repair method in the form of a subset of repair quantities (Qs). Once the Qs have been established for a given scenario, the total repair costs can be generated through a unit cost function (Figure 16), and an estimate of the repair effort can be obtained through a production rate for each Q (Mackie et al. 2008, 2010).

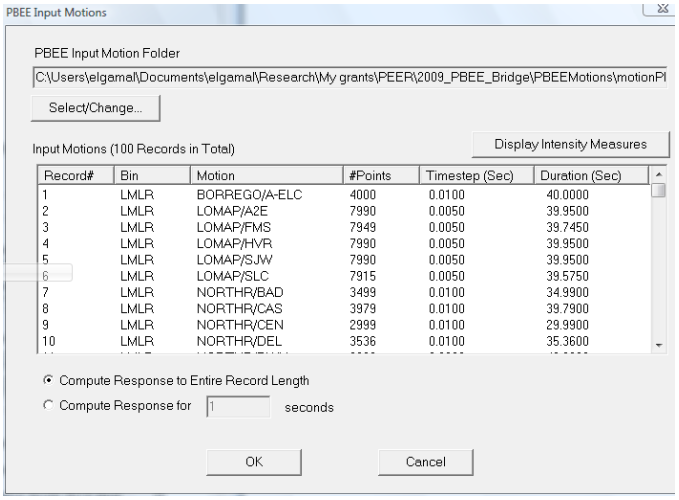

Figure 14. Ground motion selection screen.

LIQUEFACTION

I. Cyclic Mobility

In saturated clean medium-to-dense cohesionless soils, liquefaction-induced shear deformation is observed to accumulate in a cycle-by-cycle pattern (cyclic mobility). Much of the shear strain accumulation occurs rapidly during the transition from contraction to dilation (near the phase transformation surface) at a nearly constant low shear stress and effective confining pressure. Such a stress state is difficult to employ as a basis for predicting the associated magnitude of accumulated permanent shear strain.

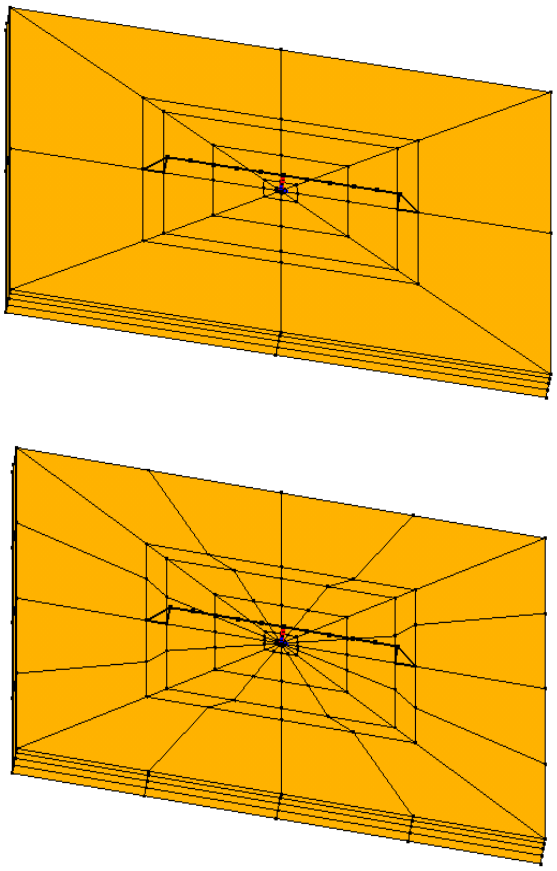

Figure 15. Bridge-foundation-ground meshes.

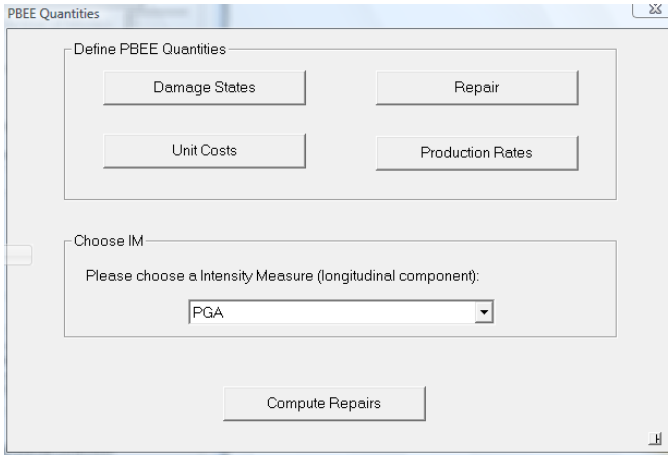

Figure 16. PBEE quantity user interface.

As such, a more convenient approach was developed (Yang 2000, Elgamal et al. 2003, Yang et al. 2003) in which the domain of large shear strain is directly defined by strain space parameters (Figures 17, 18). A calibration phase was also undertaken based on data from laboratory sample tests and dynamic centrifuge experiments (for Nevada sand at a relative density of about 40%). Recently, this multi-yield surface Mises-type constitutive model was extended (Yang and Elgamal 2008) to the more accurate Lade-Duncan Formulation (Figure 19).

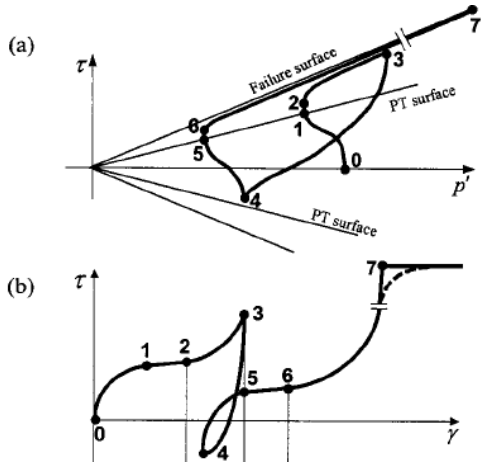

Figure 17. Schematic of constitutive model response showing octahedral stress versus effective confinement, and shear stress strain response (Yang et al. 2003).

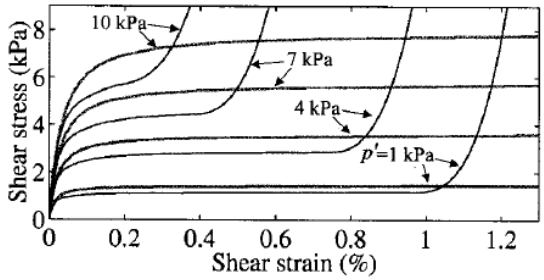

Figure 18. Comparison between undrained and drained monotonic simple shear stress-path (Yang et al. 2003).

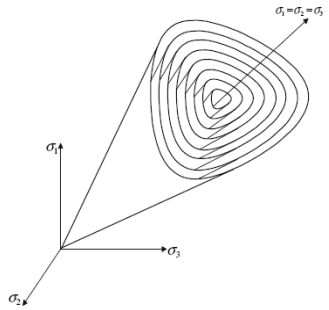

Figure 19. Configuration of Lade-Duncan multi-yield surface formulation in principal-stress space (Yang and Elgamal 2008).

II. Saturated dense sand behavior

A highly instrumented centrifuge experiment was conducted at the Univ. of California at Davis, to investigate the seismic response of a saturated dense sand stratum (Elgamal et al. 2005). Nevada sand at about 100% relative density was employed in a laminated (flexible shear beam) container to simulate one-dimensional site response. Among the total of 27 imparted earthquake-like shaking events, peak accelerations near ground surface ranged from 0.03 to 1.7g (in prototype scale), covering linear to highly nonlinear scenarios. This comprehensive set of recorded downhole accelerations was utilized to identify variation of shear modulus and damping ratio with shear strain amplitude.

The estimated modulus reduction and damping ratio (Fig. 20) displayed a confinement dependence (Figs. 21, 22). At shear strains below about 0.2%, modulus variation was found in reasonable agreement with the formulae of Hardin–Drnevich and the modulus reduction bounds of Seed–Idriss, while damping was generally higher. At shear strains larger than 0.2%, the shear-induced dilation tendency maintained secant shear modulus at about 20% of its initial value, with a 20% damping ratio approximately (Fig. 21, 22). Based on the findings, a two-phase (solid and fluid) fully-coupled nonlinear finite element program was calibrated and used to conduct numerical simulations of representative weak to strong shaking events. The computational results were in good agreement with the recorded counterparts, and satisfactorily reproduced the salient dilation effects (Figs. 20-22).

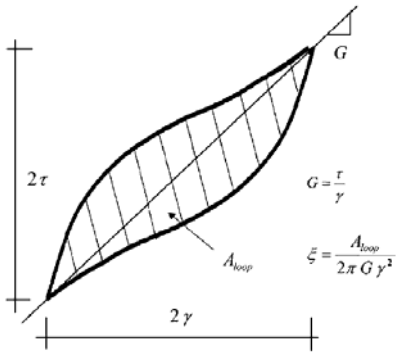

Figure 20. Schematic for evaluation of shear modulus and damping ratio from shear stress strain loop (Elgamal et al. 2005).

III. Influence of Permeability

Permeability of a liquefiable soil profile may affect the rate of pore-pressure buildup and subsequent dissipation during and after earthquake excitation (Yang and Elgamal 2002). Consequently, effective soil confinement and available resistance to shear deformations may be significantly dependent on permeability in many practical situations (Fig.

23). If present, spatial variation in permeability may even have a more profound impact on available overall shear resistance. In such situations, the onset of liquefaction-induced densification may result in water or water-rich thin inter-layers trapped below overlying low-permeability strata. The presence of these low-shear-strength inter-layers (Fig. 24) may trigger excessive (or even unbounded) localized shear deformations (flow failure mechanism).

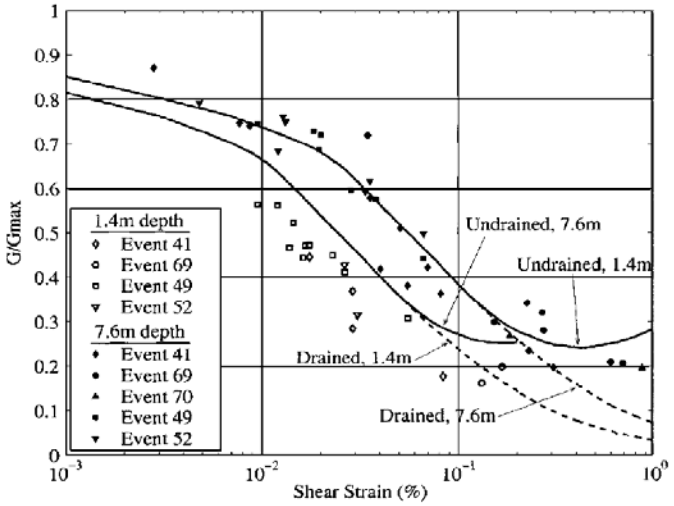

Figure 21. Model generated modulus reduction curves at different depths for saturated sends Nevada sand (D_r approx. 100%) and data points from centrifuge experiment (Elgamal et al. 2005).

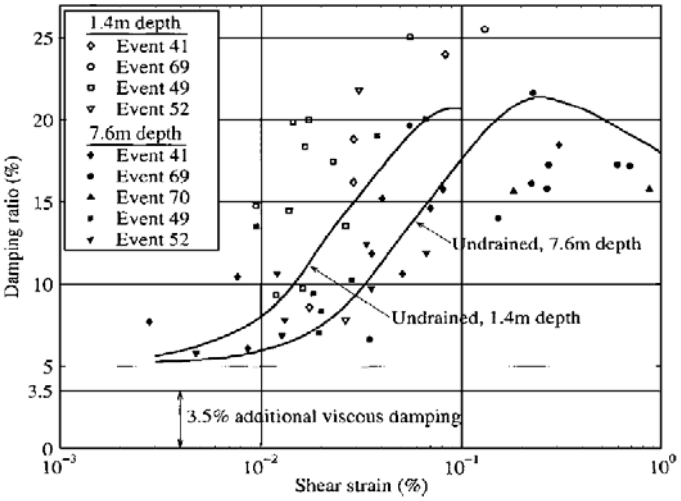

Figure 22. Overall model damping (including 3.5% viscous damping) at different depths for saturated sense Nevada sand (D_r approx 100%) and data points from centrifuge experiment (Elgamal et al. 2005).

In Yang and Elgamal (2002), numerical modeling was employed to investigate the influence of permeability and the spatial variation thereof on liquefaction-induced shear deformations. The involved response characteristics were numerically simulated using a fully coupled two-phase (solid–fluid) FE program.

The reported studies aimed to shed light on: 1) the potential significance of permeability in liquefaction-induced shear deformation assessments, 2) the importance of field investigations and research related to quantification of overall site permeability profiles, and 3) the role of relatively impervious narrow seams or inter-layers in the possible development of a catastrophic flow failure mechanism. Such situations abound in liquefiable natural (e.g., alluvial) as well as man-made (e.g., hydraulic-fill) soil deposits (Yang and Elgamal 2002).

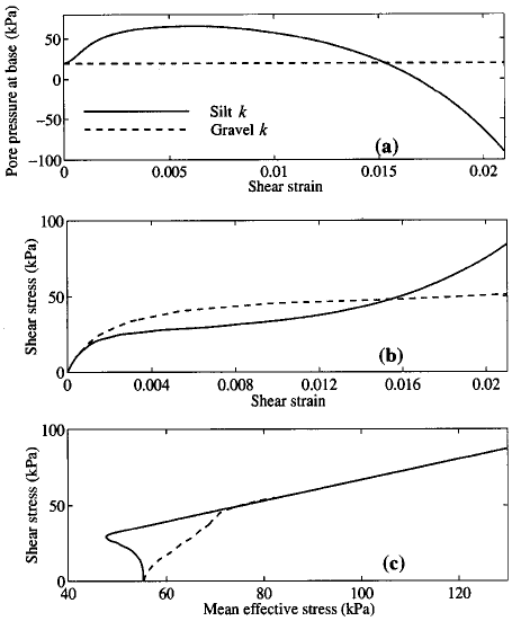

Figure 23. Monotonic loading pore-pressure, shear stress-strain and effective stress for soil with gravel versus silt permeability (Yang and Elgamal 2002).

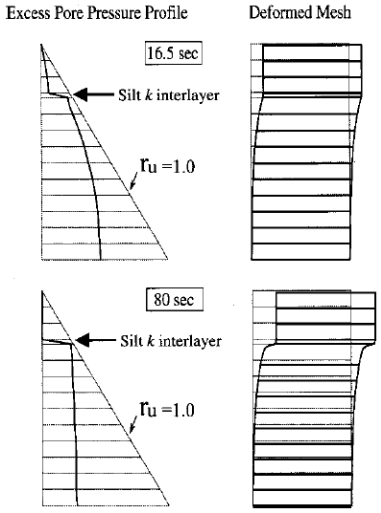

Figure 24. Excess pore-pressure profile and deformed mesh: clean sand soil profile with a silt permeability k interlayer (Yang and Elgamal 2002).

IV. Simulation of Liquefaction Countermeasures

In light of the above liquefaction response characteristics, studies were undertaken (using OpenSeesPL) to explore the mitigation of lateral spreading by stone columns and the pile-pinning effect (Elgamal et al. 2009). In a remediated area of large spatial extent (Figure 25), the periodic boundary technique (Law and Lam 2001) offers an effective approach for conducting 3D analyses (i.e., symmetry allows the investigation of a representative remediated "cell"). On this basis, Elgamal et al. (2009) conducted a 3D FE ground modification parametric study, to evaluate mitigation of liquefaction-induced lateral soil deformation by the stone column and the pile pinning approaches (Figure 25).

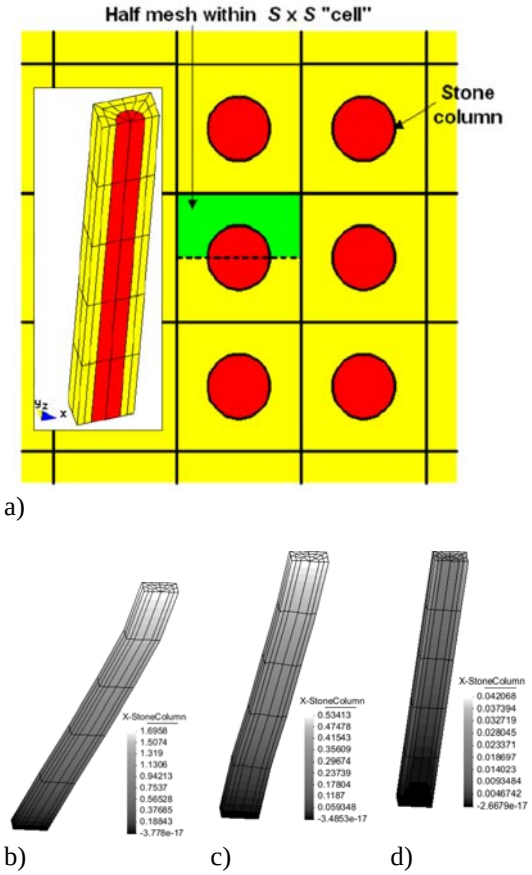

Figure 25. Ground modification study for mitigation of liquefaction-induced lateral deformation: a) cellular ground modification and FE mesh (1/2 mesh due to symmetry); b) - d) final deformed mesh for cases of medium silt, 20% stone-column replacement ratio, and pile-pinning effect, respectively (factor of 5; contour fill shows longitudinal displacement in meters).

Using OpenSeesPL, a half-mesh was studied due to symmetry (Figure 25), with the fully-coupled effective-stress plasticity-based formulation. A 10 m depth mildly-inclined (4 degrees) saturated layer was analyzed, with the remediated zone diameter maintained at 0.6 m throughout. Liquefaction-induced lateral deformation and remediation procedures for mildly sloping sand and silt strata were investigated under the action of an applied earthquake excitation. The extent of deployed remediation (area replacement ratio) and effect of the installed stone column permeability were analyzed. Effect of lateral spreading on the pile response was also investigated (Elgamal et al. 2009).

SUMMARY AND CONCLUSIONS

Three-dimensional simulation of combined ground-foundation-structural systems was shown to yield valuable insights. For instance, the influence of seismically-induced ground deformation on the overall structural response of a large bridge was highlighted. For pile-supported wharf structures, pile-pinning effects and the resulting pile deformation pattern were also addressed.

To facilitate the execution of 3D simulations, developments related to a graphical user interface (OpenSeesPL, http://cyclic.ucsd.edu/opneseespl) were outlined. From an OpenSeesPL-generated lateral push-over analysis of a large pile group, it was shown that corner piles shoulder a relatively high overall level of stresses (axial, shear, and bending). At high levels of lateral deformation, substantial axial stresses may develop that would then warrant careful consideration.

For liquefaction-induced ground deformation, the mechanism of cyclic mobility and the role of permeability were discussed. Results of pertinence to dense sand were presented in terms of the relationship between shear strain and shear modulus/ equivalent viscous damping. Incorporation of such mechanisms (http://cyclic.ucsd.edu/openseespl) for 3D analysis of liquefaction-induced lateral ground deformation countermeasures was finally discussed.

ACKNOWLEDGMENTS

The author is grateful for the funding provided by the Pacific Earthquake Engineering Research (PEER) Center under NSF Award Number EEC-9701568, the PEER Lifelines program, and the NSF Grants No. CMMI-0529995 and OCI-0749227.

APPENDIX

The employed FE analysis platform OpenSees http://opensees.berkeley.edu) includes a large library of element and material models that are particularly suited to earthquake engineering simulation (Mazzoni et al. 2006). Among the main capabilities accessible via the user interface OpenSeesPL are:

1) Solid elements and soil models

For the soil domain, 3D brick elements are included in OpenSees with coupled solid-fluid capabilities (Yang 2000, Yang and Elgamal 2002), following the original *u-p* formulation (Chan 1988), in which *u* is displacement of the soil skeleton, and *p* is pore pressure. This implementation is based on the following assumptions: small deformation and rotation, solid and fluid density remain constant in both time and space, porosity is locally homogeneous and constant with time, soil grains are incompressible, and solid and fluid phases are accelerated equally.

In addition, multi-yield surface soil models (Yang 2000, Yang et al. 2003) are available for the pressure-independent (J_2 plasticity) and pressure-dependent Drucker-Prager scenarios (Figure 26). The pressure-dependent (Yang and Elgamal 2002; Elgamal et al. 2003) was developed based on the multi-surface-plasticity theory for frictional cohesionless soils proposed by Prevost (1985). This model was developed with emphasis on simulating the liquefaction-induced shear strain accumulation mechanism in clean cohesionless soils (Yang and Elgamal 2002; Elgamal et al. 2003). The above soil elements and models allow for simulation of dry/fully saturated soil conditions.

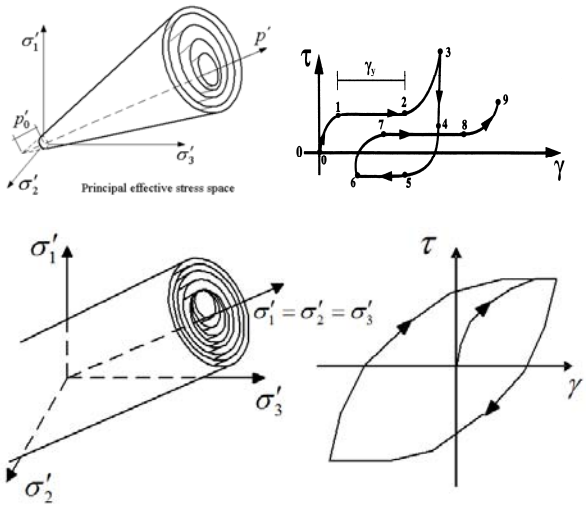

Figure 26. Multi-yield surface soil models available in OpenSees (J_2 and Drucker-Prager).

2) Beam-column elements

In OpenSeesPL, the OpenSees beam-column linear, bilinear and fiber force-based elements may be directly accessed (Spacone et al. 1996, De Sousa 2000, McKenna and Fenves 2001). For the fiber element, the uni-axial Kent-Scott-Park model (Kent and Park 1971, Scott et al. 1982, Mander et al. 1988) with degraded linear unloading/reloading stiffness is used to model the concrete (Figure 27). The reinforcing steel is represented by a uni-axial bilinear inelastic model with kinematic hardening (equivalent to a 1-D J_2 plasticity model with linear kinematic hardening) as shown in Figure 28.

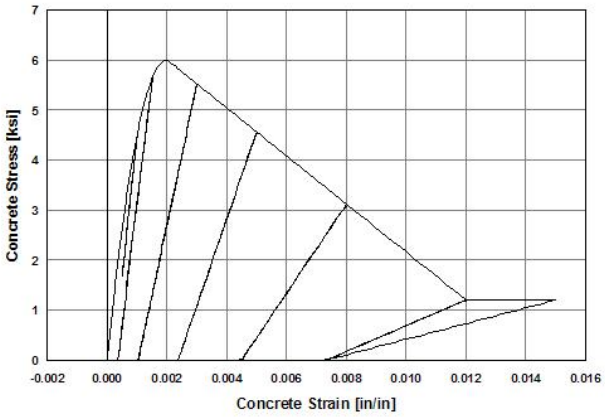

Figure 27. Concrete Kent-Scott-Park model with degraded linear unloading/reloading stiffness (Mazzoni et al 2006).

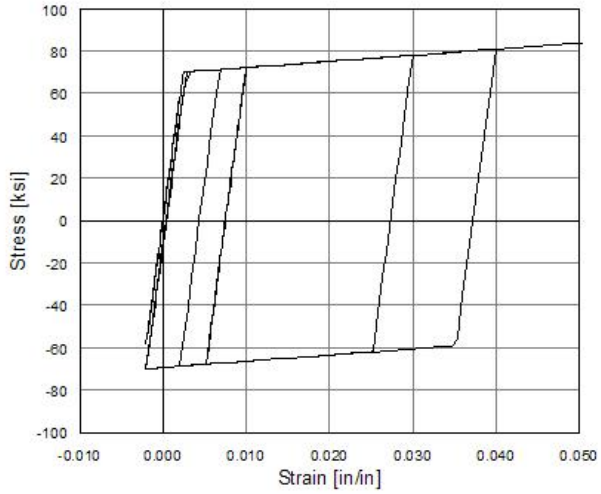

Figure 28. Steel bilinear inelastic model with linear kinematic hardening (Mazzoni et al 2006).

REFERENCES

Abedzadeh, F., and Pak, Y.S. 2004. Continuum mechanics of lateral soil–pile interaction. *Journal of Engineering Mechanics*, 130(11): 1309-1318.

Chan, A.H.C., 1988. A unified finite element solution to static and dynamic problems in geomechanics, PhD Thesis, University College of Swansea, U. K.

De Sousa, R. M. 2000. Force-based finite element for large displacement inelastic analysis of frames, *Ph.D. Dissertation*, University of California, Berkeley.

Elgamal, A., Yang, Z., Parra, E., and Ragheb, A. 2003. Modeling of cyclic mobility in saturated cohesionless soils. *International Journal of Plasticity*, 19(6), 883-905.

Elgamal, A., Yang, Z., Lai, T., Wilson, D., and Kutter, B. 2005. Dynamic response of saturated dense sand in laminated centrifuge container, *Journal of Geotechnical and Geo-environmental Engineering*, ASCE, Vol. 131, No. 5, May.

Elgamal, A., Yan, L., Yang, Z. and Conte, J. P. 2008. Three-dimensional seismic response of bridge foundation-ground system, *Journal of Structural Eng*, ASCE, Vol. 134, No. 7, July, 1165-1176.

Elgamal, A., and Lu, J. 2009. A framework for 3D finite element analysis of lateral pile system response, Proceedings of the 2009 International Foundation Congress and Equipment Expo, Contemporary Topics in In Situ Testing, Analysis, and Reliability of Foundations, ASCE GSP 186, M. Iskander, D.F. Laefer, and M.H. Hussein, Eds, Orlando, Florida, March 15–19, pp. 616-623.

Elgamal, A. Lu, J., and Forcellini, D. 2009. Mitigation of liquefaction -induced lateral deformation in a sloping stratum: 3D numerical simulation, *Journal of Geotechnical and Geoenvironmental Engineering*, 135(11), 1672-1682.

Kent, D. C., and Park, R. 1971. Flexural members with confined concrete, *J. Structural Engineering Division., ASCE*, 97(7), 1969–1990.

Law, H. K. and Lam, I. P. 2001. Application of periodic boundary for large pile group, *J. Geotech. Geoenviron. Eng.*, ASCE, 127, 10, 889–892.

Lu, J. 2006. Parallel finite element modeling of earthquake site response and liquefaction, *PhD Thesis*, Department of Structural Engineering, University of California, San Diego, La Jolla, CA.

Lu, J., Yang, Z., and Elgamal, A. 2006. OpenSeesPL three-dimensional lateral pile-ground interaction version 1.00 user's manual, *Report No. SSRP-06/03*, Department of Structural Engineering, University of California, San Diego, La Jolla, CA.

Lu, J., Elgamal, A., Sikorsky, C. and Shantz, T. 2010. Computational modeling of a large pile group under lateral load, *Proc. 5th Intl. Conf. on Recent Advances In Geotechnical Earthquake Engineering and Soil Dynamics*, and Symposium in Honor of Prof. I.M. Idriss, May 24-28, San Diego, CA (to appear).

Mackie, K.R., Wong, J-M., and Stojadinovic, B. 2008. Integrated Probabilistic Performance-Based Evaluation of Benchmark Reinforced Concrete Bridges, Report No. 2007/09, Pacific Earthquake Engineering Research Center, University of California, Berkeley.

Mackie, K.R., Wong, J-M., and Stojadinovic, B. 2010. Post-earthquake bridge repair cost and repair time estimation methodology. *Earthquake Engineering & Structural Dynamics*, Volume 39 Issue 3, Pages 281 - 301.

Mander, J. B.,.Priestley, M. J. N and Park, R. 1988. Theoretical Stress-Strain Model for Confined Concrete, *Journal of the Structural Engineering*, 114(ST8), 1804-1826.

Mazzoni, S., McKenna, F., and Fenves, G. L. 2006. Open system for earthquake engineering simulation user manual, Pacific Earthquake Engineering Research Center, University of California, Berkeley (http://opensees.berkeley.edu/).

McKenna, F. T., and Fenves, G. L. 2001. *The OpenSees Command Language Manual, Version 1.2*, Pacific Earthquake Engineering Research Center, University of California, Berkeley.

Prevost, J.H. 1985. A simple plasticity theory for frictional cohesionless soils. *Soil Dynamics and Earthquake Engineering*, 4(1), 9-17.

Scott, B. D., R. Park, and Priestley, M. J. N. 1982. Stress-strain behavior of concrete confined by overlapping hoops at low and high strain rates, *ACI Journal*, 79(1), 13-27.

Spacone, E., Filippou, F. C. and Taucer, F. F. 1996. Fibre beam-column model for non-linear analysis of r/c frames: part I. formulation, *Earthquake Eng and Structural Dynamics*, 25(7), 711-725.

Yan, L., 2006. Sensor data analysis and information extraction for structural health monitoring, *Ph.D. dissertation*, Univ. of California, San Diego, Dept. of Structural Eng, La Jolla, CA.

Yang, Z. 2000. Numerical modeling of earthquake site response including dilation and liquefaction, *PhD Thesis*, Department of Civil Eng and Eng Mechanics, Columbia University, NY, NY.

Yang, Z. and Elgamal, A. 2002. Influence of permeability on liquefaction-induced shear deformation, *Journal of Engineering Mechanics*, ASCE, 128(7), 720-729.

Yang, Z., Elgamal, A., and Parra, E. 2003. A computational model for cyclic mobility and associated shear deformation, *Journal of Geotechnical and Geoenvironmental Engineering*, 129(12), 1119-1127.

Yang, Z., Lu, J. and Elgamal, A. 2004. A web-based platform for computer simulation of seismic ground response, *Advances in Engineering Software*, 35(5), 249-259.

Yang, Z. and Elgamal, A. 2008. Multi-surface cyclic plasticity sand model with Lode angle effect, Journal of Geotechnical and Geological Engineering, Vol. 26, No. 3, 3350348, Springer Netherlands, June.

Zhang, Y., Conte, J. P., Yang, Z., Elgamal, A., Bielak, J., and Acero, G. 2008. “Two-dimensional nonlinear earthquake response analysis of a bridge-foundation-ground system,” *Earthquake Spectra*, Vol. 24, No. 2, May, 343-386.